



The cool-down behaviour of a miniature Joule–Thomson (J–T) cryocooler with distributed J–T effect and finite reservoir capacity



R.M. Damle, M.D. Atrey*

Refrigeration and Cryogenics Laboratory, Department of Mechanical Engineering, Indian Institute of Technology Bombay, Powai, Mumbai 400076, Maharashtra, India

ARTICLE INFO

Article history:

Received 10 February 2015
 Received in revised form 14 May 2015
 Accepted 16 May 2015
 Available online 23 May 2015

Keywords:

J–T cryocooler
 Cool-down
 Reservoir capacity
 Heat-exchanger

ABSTRACT

The objective of this work is to study the effect of the reservoir pressure and volume on the cool-down behaviour of a miniature Joule–Thomson (J–T) cryocooler considering the distributed J–T effect. As the supply pressure to the J–T cooler reduces in case of a reservoir with finite capacity, the volume and the initial pressure of the reservoir are crucial for the operation of the cryocooler. These parameters affect the cool down time, cooling effect and the time for which the cooling effect is obtained at the required cryogenic temperature. A one dimensional transient model is formulated for the fluid streams and the solid elements of the recuperative heat exchanger of the cryocooler. Argon gas is used as the working fluid and its physical properties are evaluated at the local conditions of temperature and pressure. Cases with different reservoir capacities and pressures are worked out to study their effect on the transient behaviour of the cryocooler.

© 2015 Elsevier Ltd. All rights reserved.

1. Introduction

The Joule–Thomson effect, production of cold by expanding a high pressure gas, was discovered by William Thomson and Prescott Joule with their porous plug experiment in 1853 [1]. Ever since its discovery, cooling to cryogenic temperatures with Joule–Thomson (J–T) effect is one of the most widely known and experimented methods. Miniature J–T cryocoolers have advantages like: simple design; no moving parts; high reliability; less maintenance; and low cost. Also, with the typical supply pressures in the range of 200–400 bar, the cool down time for miniature J–T cryocoolers can be less than a minute. Moreover, the possibility of miniaturization is well suited for applications like thermal cameras, cryosurgery probes, cooling of infrared sensors etc. The most critical element of such cryocoolers is the counter flow recuperative heat exchanger. The recuperative heat exchanger, typically of Hampson type as shown in Fig. 1, consists of a finned tube wound over a mandrel core and a covering shield forming an outer annulus. In an open cycle mode, the high pressure gas from the reservoir flows through the finned tube, expands through an orifice/expansion device, and flows over the outer finned tube surface cooling the high pressure gas before going out to the surroundings. The geometrical configuration and the operating conditions directly affect the performance of the cryocooler in terms of cooling

capacity and cool down time. In the literature, various researchers have analyzed miniature Hampson type cryocoolers numerically and experimentally. Chou et al. [2] carried out transient numerical analysis and also reported experimental data for a miniature J–T cryocooler. Chien et al. [3] reported a transient model with a self-regulating bellows mechanism to regulate the mass flow rate after reaching cryogenic temperatures. Xue et al. [4] and Ng et al. [5] carried out experiments and steady state calculations for the recuperative heat exchanger with Argon gas. A steady state thermodynamic model of the miniature heat exchanger was presented by Chua et al. [6]. Hong et al. [7] conducted experiments using Nitrogen gas at inlet pressures up to 120 bar to study the transient cool down characteristics. Hong et al. [8] predicted the performance of the heat exchanger for pressures up to 500 bar with Argon and Nitrogen as working fluids. They used ϵ -NTU approach to study the performance of the heat exchanger. Ardhapukar and Atrey [9] reported a steady state analysis for the optimization of a miniature J–T cryocooler. Maytal [10] suggested that the pressure drop along the length of the high pressure side causes a distributed J–T expansion effect and any additional expansion device at the end of the finned tube could thus be eliminated. Recently, Damle and Atrey [11] investigated the distributed J–T effect. It was shown that the distributed J–T effect produces a substantial temperature drop when the pressure variation along the high pressure side is large. It should be noted that when the distributed J–T effect is considered, as suggested by Maytal [10], the changes of enthalpy and

* Corresponding author. Tel.: +91 (22)2576 7522; fax: +91 (22)2572 6875.

E-mail address: matrey@iitb.ac.in (M.D. Atrey).

Nomenclature

A	cross-sectional area, m^2
CV	control volume
C_p	specific heat, $J/kg\ K$
C_d	discharge coefficient
D_{hel}	diameter of the helix, m
d_{fi}	inner diameter of the finned tube, m
dx	CV length, m
e_r	emissivity of shield
f	fanning friction factor
G	mass velocity, $kg/m^2\ s$
h	enthalpy, J/kg
k	thermal conductivity, $W/m\ K$
l	wetted perimeter, m
L	length of the finned tube/external annulus, m
m	mass, kg
\dot{m}	mass flow rate, kg/s
Pr	Prandtl number
p	pressure, N/m^2
Re	Reynolds number
t	time, s
V	velocity, m/s
\tilde{V}_r	volume of reservoir, m^3
x	distance in positive x -direction, m

Greek symbols

α	heat transfer coefficient, $W/m^2\ K$
γ	ratio of specific heats of a gas
μ_{JT}	Joule–Thomson coefficient, $K\ m^2/N$
ρ	density, kg/m^3
σ	Stefan–Boltzmann constant 5.67×10^{-8} , $W/m^2\ k^4$
τ_w	wall shear stress, N/m^2

Superscripts

0	value at previous time step
---	-----------------------------

Subscripts

a, e	after expansion
amb	ambient
c	cold gas in the external annulus
h	hot gas in the finned tube
in	inlet
m	mandrel
out	outlet
s	shield
w	finned tube wall
(–)	average over CV

in turn those of temperature due to changes of pressure are also taken into account according to Eq. (1).

$$dh = C_p dT - \mu_{JT} C_p dp \quad (1)$$

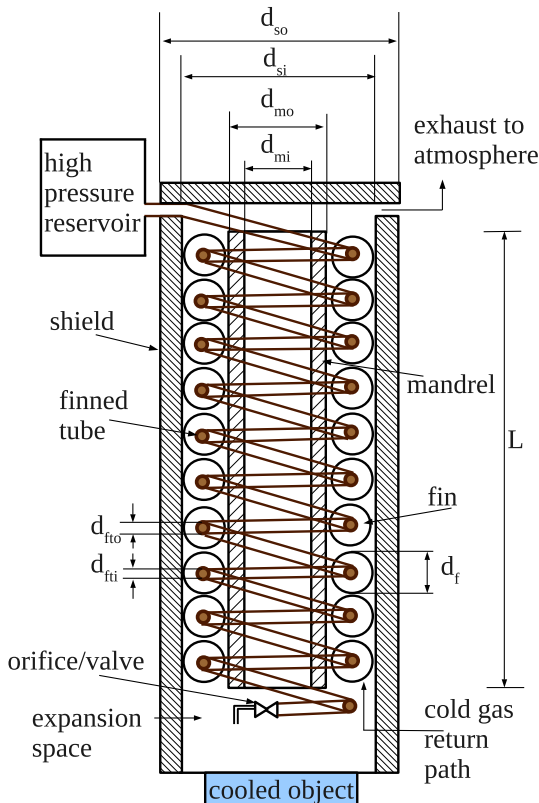


Fig. 1. Schematic of a miniature J–T cryocooler.

The contribution due to changes in pressure along the length of the finned tube, represented by the second term of the above equation, has been neglected so far in the literature. Thus, the enthalpy changes of the fluid in the finned tube have been attributed only to the changes of temperature. Moreover, all the studies mentioned above have been carried out by assuming that the pressure at the inlet of the J–T cryocooler is constant. In some applications (e.g., missile guidance systems), due to the finite capacity of the reservoir, the inlet pressure reduces because of the outflow of the working fluid. Hong et al. [12] reported a numerical study of the operating characteristics of a miniature Joule–Thomson refrigerator. They carried out numerical simulations with different volumetric capacities and initial pressures of the high pressure gas reservoir. However, the distributed J–T effect was not considered in their study. Additionally, they assumed the contribution of the transient terms in the continuity and momentum equations to be negligible. Also, the cooling effect and its variation with time were not reported in the paper. The distributed J–T effect depends on pressure drop which in turn depends on the mass flow rate. It is therefore interesting to see how the distributed J–T effect affects the transient behaviour of the cryocooler with changing reservoir pressure and the corresponding mass flow rate variation.

The objective of this work is to study the transient cool-down behaviour of the cryocooler under varying supply pressure (due to the finite capacity of the reservoir) with the distributed J–T effect along the finned tube. Numerical simulations with different starting reservoir pressures and volumetric capacities are carried out to see their effect on the cool down time and cooling effect. A one-dimensional transient model, reported previously by Damle and Atrey [11], is used for studying the transient behaviour with the distributed J–T effect. J–T expansion process at the exit of the finned tube is also simulated for completing the cryogenic process cycle. Argon gas is used as the working fluid for all the cases simulated in this work. Physical properties of Argon are evaluated at the local conditions of temperature and pressure.

Besides the distributed J–T effect, an attempt has been made to give realistic initial and boundary conditions which are crucial for

the transient evolution of the cryocooler. The mass flow rate at the exit of the finned tube is calculated for a given orifice configuration. This induces the gas flow at the inlet cross-section of the finned tube which is connected to the reservoir. Often, for the transient simulations, the initial boundary conditions are not clearly mentioned in the literature. Also, there is a lack of information about the geometrical configuration of miniature J–T cryocoolers in the literature and very few transient studies have been reported. For example, Hong et al. [12] have not specified the dimensions of the mandrel and the shield in their simulations with finite reservoir capacity. It is therefore not possible to reproduce their cases for making numerical comparisons. In the present work, geometrical configuration given by Xue et al. [4] is used for carrying out the numerical analysis. Also, the aforementioned transient model employed for simulating different cases has been verified with mesh independence exercises and validated with the experimental data of outlet temperatures given by Xue et al. [4]. In view of this, the present work may also be useful for other researchers to compare their numerical results.

2. Cryocooler configuration

A schematic of a miniature cryocooler with the recuperative heat exchanger is shown in Fig. 1. The geometrical parameters of the heat exchanger studied in this work are listed in Table 1. These are the dimensions of the miniature cryocooler reported by Xue et al. [4]. They have performed experimental and numerical analysis for the same. Usually, the high pressure gas enters the finned tube (hot side of the heat exchanger) at a pressure in the range of 100–400 bar depending on the working fluid. The temperature at the inlet is close to the ambient temperature (300 K). The gas in the helical finned tube experiences a very high pressure drop along with heat transfer. The return gas in the external annulus (cold side of the heat exchanger) enters at low pressure around 1.5–2 bar and at a temperature of about 80–110 K. The outer finned surface in the external annulus enhances the heat transfer to the return gas. The geometrical configuration of the heat exchanger (i.e., finned tube geometry, heat exchanger length, etc.) and the working conditions (i.e., mass flow rates and inlet pressure) drastically affect the cool down characteristics. A parametric study is therefore useful for optimization of the geometrical and operating parameters of the heat exchanger.

3. Mathematical model

A one-dimensional transient model is employed for the simulation of the fluid streams and the solid elements (i.e., finned tube, mandrel and shield) which together form the heat exchanger. The different elements of the heat exchanger are divided into a series of control volumes (CVs) over which the governing

equations are solved. A brief description of the previously detailed transient numerical model [11] is presented in this section.

3.1. Assumptions

The assumptions made in the derivation of the governing equations are:

- (i) heat transfer and fluid flow is one dimensional along the length of solid and fluid elements of the heat exchanger;
- (ii) axial conduction in the fluid is neglected;
- (iii) body forces and axial stresses are negligible;
- (iv) the helical tube is assumed to be perfectly circular and closely spaced;
- (v) fin efficiency is assumed to be 100%;
- (vi) inner surface of the mandrel is assumed to be adiabatic;
- (vii) emissivity of the shield is assumed to be constant and receives outside radiation at ambient temperature.
- (viii) at time $t = 0$, the initial pressure of the fluid in the finned tube is assumed to be at the reservoir pressure with closed orifice, and that of the fluid in the external annulus is assumed to be the expansion pressure.

3.2. Governing equations

The basic equations of conservation of mass, momentum and energy for the fluid elements and energy conservation equation for the solid elements are written in a differential form. The conservation of mass over a fluid CV is:

$$A \frac{\partial \bar{\rho}}{\partial t} + \frac{\partial \dot{m}}{\partial x} = 0 \quad (2)$$

The conservation of momentum is given by:

$$A \frac{\partial (\bar{\rho} \bar{V})}{\partial t} + \frac{\partial (\dot{m} V)}{\partial x} = - \frac{\partial p}{\partial x} \cdot A - \tau_w l_p \quad (3)$$

Energy equation in terms of enthalpy is written as:

$$A \frac{\partial (\bar{\rho} \bar{h})}{\partial t} + \frac{\partial (\dot{m} h)}{\partial x} = \alpha \cdot l_p \cdot (T_w - \bar{T}) \quad (4)$$

A general energy equation for the solid elements is the following:

$$\rho A C_p \frac{\partial T}{\partial t} = \frac{\partial}{\partial x} \left(k A \frac{\partial T}{\partial x} \right) + \dot{Q}_{conv} + \dot{Q}_{rad} \quad (5)$$

\dot{Q}_{conv} represents the heat transfer per unit length due to convection from the surfaces of the solid elements. \dot{Q}_{rad} is the heat transfer per unit length due to radiation considered only for the outer shield surface.

3.3. Boundary and initial conditions

The reservoir pressure reduces due to the continuous outflow of gas because of its finite capacity and the mass flow rate changes with the temperature and pressure upstream of the orifice. Therefore, for the simulations carried out in this work, in addition to the governing equations described earlier, boundary conditions changing with time are newly implemented. The mass flow rate through the orifice, estimated for a choked orifice from [13], is given by:

$$\dot{m}_{orifice} = C_d A \sqrt{\gamma p \rho} \left(\frac{2}{\gamma + 1} \right)^{(\gamma+1)/(2(\gamma-1))} \quad (6)$$

The reservoir pressures are around 80–200 bar while the expansion pressure is around 1.25–2.0 bar. These values of expansion pressure

Table 1
Dimensions of the recuperative heat exchanger (Xue et al. [4]).

Geometrical parameters	Size
Inside diameter of finned tube, d_{fi}	0.3 mm
Outside diameter of finned tube, d_{fo}	0.5 mm
Inside diameter of mandrel, d_{mi}	2.3 mm
Outside diameter of mandrel, d_{mo}	2.5 mm
Inside diameter of shield, d_{si}	4.5 mm
Outside diameter of shield, d_{so}	4.8 mm
Length of recuperative heat exchanger, L	50 mm
Fin height, h_f	0.25 mm
Fin thickness, t_f	0.1 mm
Fin density, f_d	3.3 fins/mm
Helix diameter, D_{hel}	3.5 mm
Helix pitch, P_{hel}	1 mm

are well below the critical pressure values and therefore the orifice can be considered to be under choked condition. Hong et al. [12] also carried out their study for choked orifice condition. The mass flow rate under choked condition is maximum for given upstream conditions. The choked mass flow rate calculated with Eq. (6) is valid for an ideal gas. Maytal [14] showed that the mass flow rate for a real gas under choking conditions is significantly higher than that for an ideal gas. However, the aim of this work is to understand how the distributed J–T effect affects the behaviour of the J–T cryocooler with varying mass flow rate due to the finite reservoir capacity. Therefore, choked mass flow rate of an ideal gas is assumed in this work. The value of the discharge coefficient is assumed to be 0.62 (taken according to Hong et al. [12]) and the flow area of the orifice is taken equal to 0.01 mm².

As the flow in the heat exchanger starts, the pressure in the reservoir reduces due to the continuous outflow of the gas. This pressure is calculated as a function of temperature and density of the gas in the reservoir at a given instant. The density is obtained by applying the mass conservation equation for the reservoir volume according to:

$$\frac{(\rho - \rho^0)\tilde{V}_r}{\Delta t} = -\dot{m}_{out, reservoir} \quad (7)$$

The inlet temperature and pressure of the reservoir are known for each case. The mass flow rate at the orifice is calculated from Eq. (6). This mass flow rate is set as boundary condition at the inlet of the external annulus. The corresponding pressure is given to be the pressure after expansion ($p_{c,in}$) and the temperature is set equal to the temperature after expansion ($T_{a,e}$). All the solid elements (i.e., finned tube, mandrel and shield) are assumed to be adiabatic at ends. Thus,

$$\text{at } x = 0 \text{ \& } t > 0, T = T_{h,in}, p = p_{h,in}, \frac{dT_w}{dx} = 0, \frac{dT_m}{dx} = 0, \frac{dT_s}{dx} = 0 \quad (8)$$

$$\text{at } x = L \text{ \& } t > 0, T = T_{a,e}, p = p_{c,in}, \frac{dT_w}{dx} = 0, \frac{dT_m}{dx} = 0, \frac{dT_s}{dx} = 0 \quad (9)$$

$T_{a,e}$ is the temperature of the gas after isenthalpic expansion, from its state at the exit of the finned tube, to the pressure $p_{c,in}$ in the external annulus. This temperature goes on reducing from its initial value (ambient temperature) to cryogenic temperature $T_{c,in}$ at steady state. In addition, the initial temperature map for all the solid elements is specified as:

$$\text{at } t = 0, T^0 = T_{amb} \text{ for } 0 \leq x \leq L \quad (10)$$

The initial pressure of the fluid in the finned tube is set equal to reservoir pressure ($p_{h,in}$) as:

$$\text{at } t = 0, p^0 = p_{h,in} \text{ for } 0 \leq x \leq L \text{ (finned tube)} \quad (11)$$

The initial pressure of the fluid in the external annulus is set equal to the pressure after expansion ($p_{c,in}$) as:

$$\text{at } t = 0, p^0 = p_{c,in} \text{ for } 0 \leq x \leq L \text{ (external annulus)} \quad (12)$$

Once the orifice is opens at $t > 0$, the gas flow gets induced due to the upstream pressure conditions which in turn depend on the reservoir pressure. So, the inlet pressure, mass flow rate through the orifice and the temporal evolution of cryocooler depends only on a given orifice configuration. Unlike the assumption of fixed mass flow rates and temperatures for both streams in the literature, an attempt is made in this work to give as realistic initial and boundary conditions as possible.

3.4. Heat transfer and friction factor correlations

The Fanning friction factor (f) for the flow through the helical finned tube is estimated with the correlation of Timmerhaus and Flynn [15] and is given by:

$$f = 0.184 \left(1 + 3.5 \frac{d_{fi}}{D_{hel}} \right) Re^{-0.2} \quad (13)$$

The convective heat transfer coefficient (α_h) for the turbulent flow in the finned tube, according to Timmerhaus and Flynn [15], is calculated as:

$$\alpha_h = 0.023 C_{ph} G_h Re^{-0.2} Pr^{-2/3} \left(1 + 3.5 \frac{d_{fi}}{D_{hel}} \right) \quad (14)$$

The cold gas, on its way back to the atmosphere, exchanges heat by convection with the finned surface, outer surface of the mandrel and the inner surface of the shield. The convective heat transfer coefficient (α_c) for the return flow, evaluated with the correlation from Timmerhaus and Flynn [15], is:

$$\alpha_c = 0.26 C_{pc} G_c Re^{-0.4} Pr^{-2/3} \quad (15)$$

The Fanning friction factor (f) for the flow through the external annulus is calculated according to:

$$f = 16/Re \quad Re < 2300 \quad (16)$$

$$f = 0.079 Re^{-0.25} \quad Re > 2300 \quad (17)$$

3.5. Resolution of fluid and solid elements

For resolving the governing equations, the fluid streams are divided into a series of control volumes (CVS) along their length. For the fluid in the finned tube, the pressure is known at the inlet cross-section while mass flow rate through the orifice is known at the outlet cross-section. The reservoir pressure at inlet reduces continuously and affects the mass flow rate through the orifice. Moreover, the mass flow rate values also depend on the upstream pressure and temperature of the orifice. The SIMPLEC method [16], a robust method under changing boundary conditions at either end, is therefore employed for resolving the high pressure gas flow in the finned tube. For the return stream, i.e., the gas in the external annulus, the variables (e.g. p , T , \dot{m}) are known at the inlet cross-section. Thus, an iterative step-by-step method is suitable here to obtain the variable values at subsequent cross-sections by marching in the flow direction. For the solid elements, integration of Eq. (5) over a CV results in a system of linear algebraic equations. TDMA (Tri-Diagonal Matrix Algorithm) method is used for solving this system of equations. The global resolution algorithm is detailed by Damle and Atrey [11].

4. Results and discussion

To illustrate the distributed J–T effect, cases with constant supply pressure and mass flow rates are first worked out. Thereafter, the effect of different volumetric capacities with different initial pressures of the reservoir is studied with the distributed J–T effect. The simulations are carried out with Argon as the working fluid. All the cases are simulated with the geometrical configuration of Xue et al. [4] as listed in Table 1. The physical properties of Argon are obtained from the commercial software AspenONE [17]. At any given instant, for each CV, the physical properties like density, viscosity, specific heat, thermal conductivity and enthalpy are evaluated at the local conditions of temperature and pressure. The values of thermal conductivity, as a function of temperature,

Table 2
Operating parameters of the test cases (working fluid: Argon).

$p_{h,in}$ (bar)	$T_{h,in}$ (K)	$p_{c,in}$ (bar)	T_{sat} (K)	$T_{c,in}$ (K)
80	292	1.34	89.84	100
100	292	1.34	89.84	100
140	292	1.34	89.84	100
180	292	1.72	92.48	100

for the solid elements like finned tube, mandrel and shield, are evaluated from the functions given by Ng et al. [5].

The temperature of the gas after expansion $T_{a,e}$ is given as the inlet temperature for the fluid in the external annulus. This temperature reduces from ambient temperature to $T_{c,in}$ at steady state. A minimum value of $T_{c,in}$, the inlet temperature of the gas in the external annulus, is fixed to be 100 K for the given working conditions. The cooling effect is calculated when $T_{a,e}$ falls below the $T_{c,in}$ value. The operating parameters for the simulated cases are shown in Table 2. The values of expansion pressure ($p_{c,in}$) are taken according to Ng et al. [5]. As these values should be large enough to overcome the pressure drop on the return side, they increase according to the mass flow rate for a given reservoir pressure. The saturation temperatures for each case, depending on $p_{c,in}$, are listed in Table 2. These are also the lowest attainable temperatures for the respective cases. All the cases are simulated for a physical time of 200 s as considered in the study of Hong et al. [12].

4.1. Mass flow rate and the distributed J–T effect

To study the distributed J–T effect with the mass flow rate, values of 0.37 g/s and 0.1 g/s (high and low) are chosen. Mass flow rate of 0.37 g/s represents a limiting case of choking condition, while 0.1 g/s represents a mass flow rate four times lesser than the choking value. Figs. 2 and 3, respectively, show the pressure and temperature profiles along the length of the finned tube with high pressure gas for the above mass flow rates. The results are given in both the cases with and without the distributed J–T effect. The profiles obtained without considering the distributed J–T effect are indicated with “no μ_{JT} ”. The inlet pressure is 180 bar and the temperature is 298 K. It is observed from Fig. 2 that for a low mass flow rate (0.1 g/s), the drop in pressure of the high pressure fluid in the finned tube is low (around 8 bar) for an inlet pressure of 180 bar. The pressure profiles with and without the distributed J–T effect overlap each other. This is also reflected in the temperature profiles along the length of the high pressure fluid as given in Fig. 3. This is because, when the mass flow rate is low, the pressure drop of the fluid in the finned tube is small and therefore, the

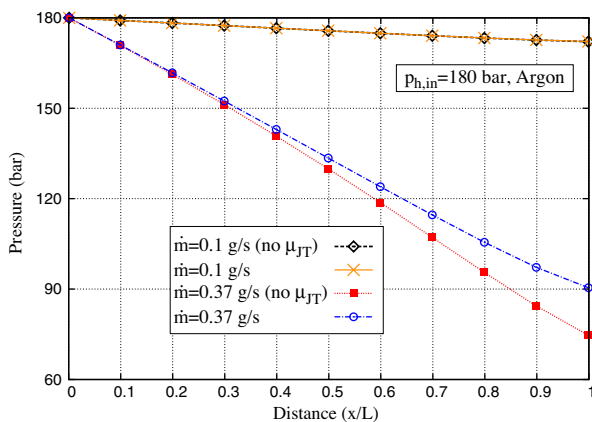


Fig. 2. Pressure along the length of the high pressure gas.

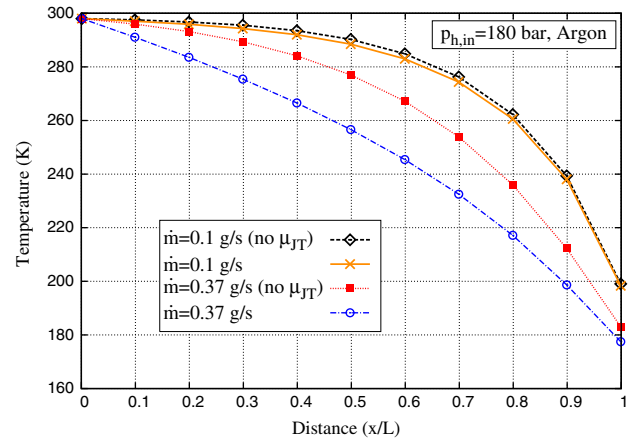


Fig. 3. Temperature along the length of the high pressure gas.

changes in temperature due to the changes in pressure (second term of Eq. (1)) are negligible. However, the profiles differ significantly when the mass flow rate increases to 0.37 g/s. As the mass flow rate increases, the pressure drop also increases. In the present case, this pressure drop is of the order of around 90–100 bar over the length of the high pressure fluid in the finned tube as can be seen from Fig. 2. Therefore, the changes in temperature due to changes in pressure, represented by the second term in Eq. (1), become significant. This results in lower temperatures along the length of the fluid in the finned tube as shown in Fig. 3. As a result of lower temperatures, the gas density is higher and the pressure drop is lesser when the distributed J–T effect is considered. Due to higher pressure at the exit of the finned tube, the cooling effect obtained after expansion is also higher. It is clear from Figs. 2 and 3 that, depending on the mass flow rate, and in turn the pressure drop, the mathematical model captures the physics of the distributed J–T effect and its contribution to the changes in temperature along the length of the finned tube.

4.2. Effect of reservoir capacity

The effect of reservoir capacity on the transient variation of pressure, mass flow rate, cooling effect and cold end temperature is presented in this section. Different reservoir capacities varying from 100 cm³ to 500 cm³ are considered for the calculation purpose. Fig. 4 shows the variation in reservoir pressure with an initial reservoir pressure of 140 bar for various reservoir capacities. As expected, it is observed that the pressure in the reservoir drops

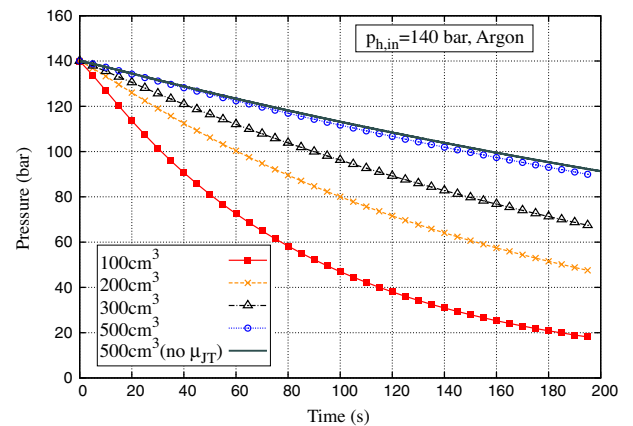


Fig. 4. Transient variation of reservoir pressure.

with time due to the continuous outflow of the gas. As the reservoir capacity increases, the slope of the curves, i.e., the rate of fall of reservoir pressure decreases. The rate of drop of the reservoir pressure is largest for the smallest reservoir with a capacity of 100 cm^3 . After 200 s, the reservoir pressure for the reservoir capacity of 100 cm^3 is around 20 bar while that for the reservoir capacity of 500 cm^3 is around 90 bar.

The drop in reservoir pressure affects the evolution of mass flow rate through the orifice and the same is shown in Fig. 5. The mass flow rate depends on the pressure and density upstream of the orifice as can be seen from Eq. (6). Initially, as the temperatures are close to ambient temperature near the cold end, there is a drop in mass flow rate due to low gas density. As cooling takes place due to continuous J–T expansion, the upstream temperatures start lowering and the mass flow rate increases due to higher gas density. Over this initial period of cool down, the pressure reduces at a lower rate than the increase of density and therefore, the mass flow rate continues to increase. For all reservoir capacities, a maximum mass flow rate, between 0.225 and 0.25 g/s, is obtained within 20 s which corresponds to the initial cool down period. After the initial cool down period, the temperatures do not vary significantly but the continuous decrease of supply pressure reduces the mass flow rate. After reaching the maximum, the mass flow rate curves are similar to the pressure curves for a given capacity. The mass flow rate drops from 0.225 g/s to 0.027 g/s for a reservoir capacity of 100 cm^3 , while the same drops from 0.25 g/s to 0.167 g/s for a reservoir capacity of 500 cm^3 .

Figs. 4 and 5 also show, respectively, the pressure and mass flow rate variation for the reservoir capacity of 500 cm^3 without the distributed J–T effect. The same is indicated with “no μ_{JT} ”. It is seen that the mass flow rates are lower without considering the distributed J–T effect. This is due to the fact that the density of the gas is lower due to higher temperatures on the high pressure side, in case of “no μ_{JT} ” consideration, as shown in Fig. 3. Due to relatively low mass flow rates, the rate of drop of reservoir pressure is also low when the distributed J–T is not considered as can be seen in Fig. 4. The above trends in the transient evolution of pressures and mass flow rates are similar for different initial pressures of the reservoir.

Fig. 6 shows the cold end temperature variation with time for different reservoir capacities. The initial reservoir pressure is kept as 140 bar. Here also, the effect of not considering the distributed J–T effect is shown for the reservoir capacity of 500 cm^3 . It is observed that the initial cool down time (around 6 to 8 s) does not vary significantly with the reservoir capacity and the lowest temperature of about 90 K is obtained for all the cases. However, as the reservoir capacity reduces from 500 cm^3 to 100 cm^3 , the

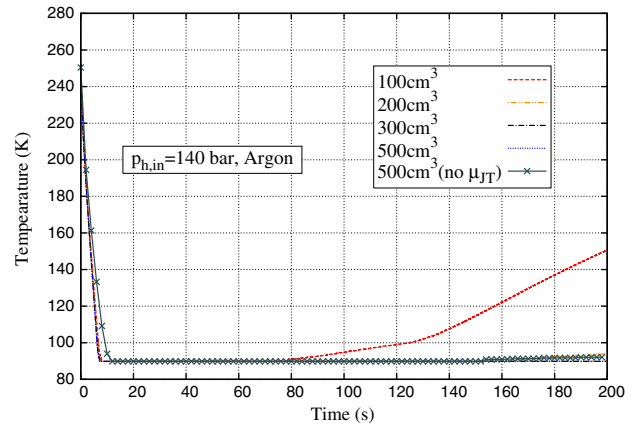


Fig. 6. Transient variation of the cold end temperature.

time for which the cold end temperature remains below 100 K decreases. For a reservoir capacity of 100 cm^3 , after 80 s, the cold end temperature starts increasing. After 125 s, it goes beyond 100 K due to the decrease of supply pressure and in turn the mass flow rate. The cold end temperature remains below 100 K for 200 s for the reservoir capacities of 200 cm^3 and above. When the distributed J–T effect is not considered, the initial cool down time increases to 12 s but the cold end temperature is maintained below 100 K for the simulation period of 200 s.

The cooling effect obtained at 100 K is shown in Fig. 7. Cooling effect without considering the distributed J–T effect is also plotted in this figure. In normal experiments on cryocoolers, for obtaining cooling load maps, the cooling load is applied when the lowest temperature is obtained and the cryocooler operation reaches a steady state. However in the present study, the cool-down behaviour of the J–T cryocooler is studied for a reservoir which has finite capacity, wherein, the pressure and mass flow rate reduce continuously with time. The cryocooler, therefore, never reaches a steady state. Therefore, in the simulation study, the cooling load at 100 K is calculated as soon as the cryocooler reaches temperature less than 100 K.

The cooling effect obtained at 100 K increases initially due to the increase in mass flow rate. This increase in cooling effect increases with reservoir capacity due to corresponding increase of mass flow rate as pointed out earlier in Fig. 5. With time, due to decrease in the mass flow rate, the cooling effect decreases. The rate of decrease of cooling effect is higher for smaller reservoir capacities. This is because the reservoir pressure and therefore the

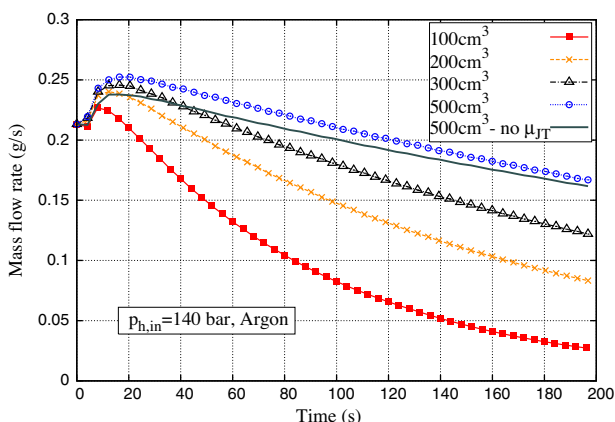


Fig. 5. Transient variation of mass flow rate.

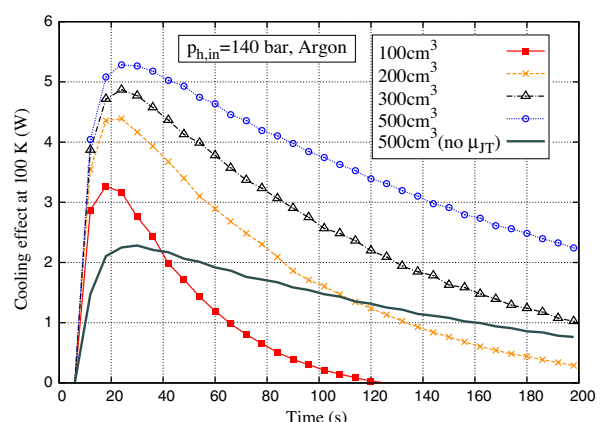


Fig. 7. Transient variation of the cooling effect at 100 K.

mass flow rates drop at a higher rate for small reservoir capacities. It is also seen from Fig. 7 that the cooling effect at 100 K remains well above 1 W and 2 W for the reservoir capacities of 300 cm³ and 500 cm³ respectively. The corresponding values of maximum cooling effect are 4.86 W and 5.28 W respectively. Without the distributed J–T effect, for reservoir capacity of 500 cm³, the maximum cooling effect reaches a value of 2.28 W at 100 K. In this case, the cooling effect stays above 1 W for up to 160 s. Also, the rate of decrease of cooling effect is gradual as compared to the case with the distributed J–T effect. This is explained by the relatively low mass flow rates without distributed J–T effect which lead to a slow decay of the reservoir pressure.

In view of the observations from Figs. 2 and 3, it may be noted that the distributed J–T effect is significant during the initial cool-down period. During this period, due to high mass flow rates the cooling effects are also high as shown in Figs. 5 and 7 respectively. It is observed that the cooling effect at 100 K is well above 1 W over the entire period of 200 s for reservoir capacities of 300 cm³ and 500 cm³. This highlights the role of a variable orifice opening in a miniature J–T cryocooler. If the orifice is regulated properly, a cooling effect of 1 W at 100 K can be maintained for much longer periods than the period of simulation in this study.

4.3. Effect of reservoir pressure

The earlier section highlighted the effect of reservoir capacity on the cool down behaviour for a fixed initial pressure of the reservoir. In this section, the effect of variation in initial reservoir pressure for a given volumetric capacity is presented. For a given reservoir volume, the initial pressure of the reservoir affects the rate at which the mass flows in the heat exchanger and therefore influences the cool down characteristics. Fig. 8 shows the cold end temperature for the reservoir capacity of 100 cm³ which is the smallest volume studied in this work. With an initial reservoir pressure of 80 bar, the cold end temperature does not fall below 100 K (comes closer to 130 K and increases thereafter). As the reservoir pressure increases from 100 to 180 bar, the cold end temperature falls below 100 K and the time to obtain this temperature reduces. The lowest attainable temperatures for different initial reservoir pressures are given in Table 2. The lowest temperature is obtained in 30 s, 8.1 s and 3.8 s for reservoir pressures of 100 bar, 140 bar and 180 bar respectively. After attaining the lowest temperature the cold end temperature remains below 100 K for 100 s. Thereafter, it starts increasing even for higher pressures due to decreasing reservoir pressure.

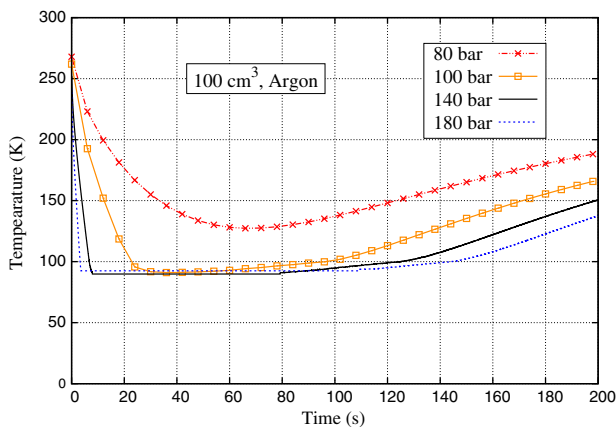


Fig. 8. Cold end temperature with time for a 100 cm³ reservoir.

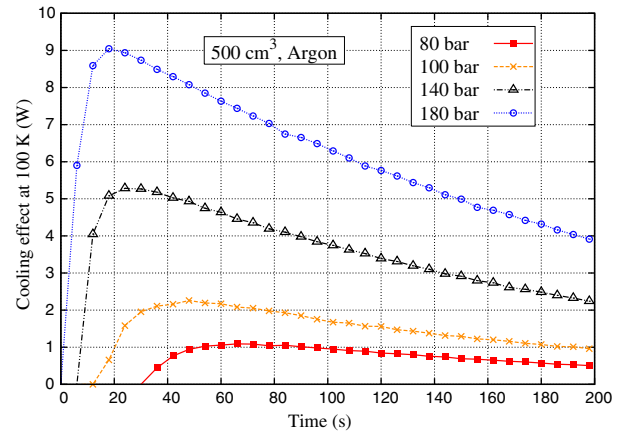


Fig. 9. Cooling effect at 100 K with time for a 500 cm³ reservoir.

It is also observed that the cold end temperature remains below 100 K with an initial reservoir pressure of 80 bar when the reservoir capacity is 300 cm³ and above. With the largest reservoir capacity (500 cm³), the lowest temperature is obtained in 42 s, 20 s, 7 s and 3.5 s with reservoir pressures of 80 bar, 100 bar, 140 bar and 180 bar respectively. In general, for all reservoir capacities, the time required for attaining the lowest temperature reduces with increase in reservoir pressure. Also, the time for which the lowest temperature is maintained below 100 K increases with increasing reservoir pressure.

Fig. 9 shows the cooling effect at 100 K for a reservoir capacity of 500 cm³. As the reservoir pressure increases, the cooling effect also increases. During the initial period, the cooling effect is more because of the high mass flow rates as seen in the earlier section. For the simulated period of 200 s, the cooling effect at 100 K is greater than 1 W, 2 W and 4 W for initial reservoir pressures of 100 bar, 140 bar and 180 bar respectively. The cooling effect reduces with time due to diminishing mass flow rates. This is true for all initial pressures of the reservoir.

It is observed that, even with the highest initial pressure (180 bar), the cooling effect falls below 1 W after 87 s and 173 s in case of reservoirs with capacities of 100 cm³ and 200 cm³ respectively. These reservoir capacities are insufficient to provide cooling effect at 100 K for longer duration. For a 300 cm³ reservoir, the cooling effect exceeds 1 W and 2 W for reservoir pressures of 140 bar and 180 bar respectively.

5. Conclusions

The cool-down behaviour of a miniature J–T cryocooler under varying reservoir pressure with distributed J–T effect is studied in this work. It is shown that, depending on the mass flow rate, the numerical model is able to regulate automatically the contribution of the distributed J–T effect. The contribution of the distributed J–T effect is significant for higher mass flow rates as the pressure drop is larger over the length of the finned tube. The cooling effect is higher when the distributed J–T effect is considered. Numerical simulations with different reservoir capacities and initial reservoir pressures have been carried out with and without considering the distributed J–T effect. When the distributed J–T effect is considered, it is seen that the cooling effect is more during the initial cool down period of high mass flow rate for finite capacity of the reservoir.

The time required to reach the lowest temperature reduces with increasing reservoir pressure, but is not affected significantly for volumetric capacities of 200–500 cm³ for a given reservoir pressure. Cooling effect is higher for higher inlet pressure and

increases with the reservoir capacity. Reservoir capacities of 100 cm³ and 200 cm³ are insufficient to maintain the cooling effect over a period of 200 s for all the initial pressures studied in this work. Cooling effect of more than 1 W at 100 K over the entire simulated period of 200 s is obtained with initial reservoir pressures of 140 bar and 100 bar for reservoir volumes of 300 cm³ and 500 cm³ respectively. Therefore, a reservoir capacity of 500 cm³ and relatively lower initial pressure of 100 bar can be used to provide cooling effect at 100 K. Any increase of initial reservoir pressure increases the cooling effect and the period over which it is obtained.

As pointed out earlier, the simulations in this work have been carried out with the choking mass flow rate for an ideal gas. It is to be noted that the choked mass flow rate values for a real gas will be higher than that for an ideal gas [14]. As observed in this work, higher mass flow rate will result in a larger distributed J–T effect and therefore will lead to more cooling effect, reduction in cool down time and faster evacuation of the reservoir. However, the qualitative trends observed here would be similar and will be studied in the future.

Finally, if the mass flow rate through the orifice is regulated after reaching the lowest temperature, the cooling effect at a given temperature can be obtained for longer periods of time than that in this work. This is another aspect about the cool-down behaviour of the cryocooler which needs attention.

References

- [1] Sittig M, Kidd S. *Cryogenics research and applications*. Princeton, New Jersey: D. Van Nostrand Company Inc; 1962.
- [2] Chou FC, Pai CF, Chien SB, Chen JS. Preliminary experimental and numerical study of transient characteristics for Joule–Thomson cryocooler. *Cryogenics* 1995;35:311–6.
- [3] Chien SB, Chen JS, Chou FC. A study on the transient characteristics of a self-regulating Joule–Thomson cryocooler. *Cryogenics* 1996;36:979–84.
- [4] Xue H, Ng KC, Wang JB. Performance evaluation of the recuperative heat exchanger in on a miniature Joule–Thomson cooler. *Appl Therm Eng* 2001;21:1829–44.
- [5] Ng KC, Xue H, Wang JB. Experimental and numerical study on a miniature Joule–Thomson cooler for steady-state characteristics. *Int J Heat Mass Transfer* 2002;45:609–18.
- [6] Chua HT, Wang X, Teo HY. A numerical study of the Hampson-type miniature Joule–Thomson cryocooler. *Int J Heat Mass Transfer* 2006;49:582–93.
- [7] Hong YJ, Park SJ, Kim HB, Choi YD. The cool-down characteristics of a miniature Joule–Thomson refrigerator. *Cryogenics* 2006;46:391–5. 46.
- [8] Hong YJ, Park SJ, Choi YD. A numerical study of the performance of a heat exchanger for a miniature Joule–Thomson refrigerator. In: *Cryocoolers 15, international cryocooler conference*; 2009. p. 379–86.
- [9] Ardhapurkar PM, Atrey M. Performance optimization of a miniature Joule–Thomson cryocooler using numerical model. *Cryogenics* 2014;63:94–101.
- [10] Maytal B-Z. Hampson's type cryocoolers with distributed Joule–Thomson effect for mixed refrigerants closed cycle. *Cryogenics* 2014;61:92–6.
- [11] Damle RM, Atrey MD. Transient simulation of a miniature Joule–Thomson (J–T) cryocooler with and without the distributed J–T effect. *Cryogenics* 2015;65:49–58.
- [12] Hong YJ, Park SJ, Choi YD. A numerical study on operating characteristics of a miniature Joule–Thomson refrigerator. *Supercond Cryogenics* 2010;12(4):41–5.
- [13] Crowe CT, Elger DF, Roberson JA. *Engineering fluid mechanics*. 7th ed. New York: John Wiley; 2001.
- [14] Maytal B-Z. Real gas choked flow conditions at low reduced-temperatures. *Cryogenics* 2006;46:21–9.
- [15] Timmerhaus KD, Flynn TM. *Cryogenic process engineering*. New York, USA: Plenum press; 1989.
- [16] Patankar SV. *Numerical heat transfer*. Hemisphere publishing corporation; 1980.
- [17] AspenONE V 7.1. Burlington, MA 01803, USA: Aspen Technology Inc; 2009.